Investigation on Maximizing Power Transfer Efficiency of Wireless In-wheel Motor by Primary and Load-Side Voltage Control

Gaku Yamamoto*a) Student Member, Takehiro Imura*b) Member
Hiroshi Fujimoto*c) Senior Member

The authors have been developed a Wireless Power Transfer (WPT) system for the In-Wheel Motor (IWM). It is called the Wireless In-Wheel Motor (W-IWM). This paper presents the way in which the efficiency of WPT is enhanced in this system. Some methods which maximize power transfer efficiency by power converter control have been proposed in the past WPT research. In these research projects, a DC-DC converter is inserted on the receiver side to vary the load state. However, space on the receiver side is so small for the W-IWM, and it is preferable to make the secondary circuit small. Therefore, a full bridge converter is used instead of a DC-DC converter in the W-IWM. In this paper, the authors propose a theoretical formula for the transfer efficiency of the W-IWM. And, from analysis of the formula, we indicate that there is a combination of the primary voltage and the load voltage which maximizes the efficiency. The feasibility is validated by an experiment using a motor bench set.

Keywords: wireless power transfer, magnetic resonance coupling, in-wheel motor, electric vehicle, efficiency

1. Introduction

Recently, Electric Vehicles (EV) have been attracting much attention. EVs are not only environmentally friendly but are also easier for motion control. By using motors as sources of its driving force, EVs have a faster response time than engine vehicles [(1)]. Moreover, a structure in which a motor is in a wheel can be achieved because a motor can be made to be smaller than an engine. This is called an In-Wheel Motor (IWM). IWM have many advantages because they can control each wheel independently and is space efficient [(2)]. However, since IWMs are under the suspension system, the power and signal lines can be broken by repeated bending. In order to solve this problem, new structures have been considered to enhance the durability of the cable [(3) (4)]. However, all methods use cables, and therefore, the problem cannot be solved.

Therefore, the authors have been developing Wireless Power Transfer (WPT) system for IWM [(5)~(7)]. Coils and a radio communication device are placed on board and in-wheel. Then, electric power and information are transferred to the IWM wirelessly. Therefore, no cables are needed between the body and the IWM. Moreover, if WPT to a moving vehicle is achieved in the future, coils buried under the ground can be used for WPT to the IWM. The authors call this system the Wireless In-Wheel Motor (W-IWM). Relative position of coils will change because of the suspension stroke in the IWM. Hence, wireless power transfer via magnetic resonant coupling, which is robust to shift in position, is applied [(8) (9)].

a) Correspondence to: yamamoto@hflab.k.u-tokyo.ac.jp
b) Correspondence to: imura@hori.k.u-tokyo.ac.jp
c) Correspondence to: fujimoto@k.u-tokyo.ac.jp
* The University of Tokyo
5-1-5, Kashiwanoha, Kashiwa, Chiba, 227-8561 Japan

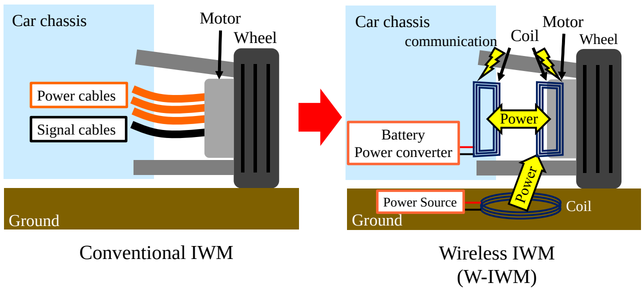

Fig. 1. W-IWM image

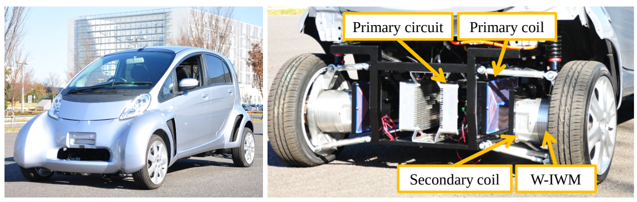

(a) FPEV4-*Sawyer* (b) First trial unit

Fig. 2. Experimental EV and first trial unit

It is known that efficiency of WPT changes based on the state of the load. Some methods which maximize power transfer efficiency by power converter control are proposed in past WPT research [(10)~(12)]. In such research, a DC-DC converter is inserted on the receiver side to vary the load state. And a diode bridge is used as an AC-DC converter. However, space of the receiver side is so small for the W-IWM that it is preferable to make the secondary circuit small. Moreover, the rectifier on the receiver side is used as an inverter in the case where the IWM regenerates. Therefore, a full bridge con-

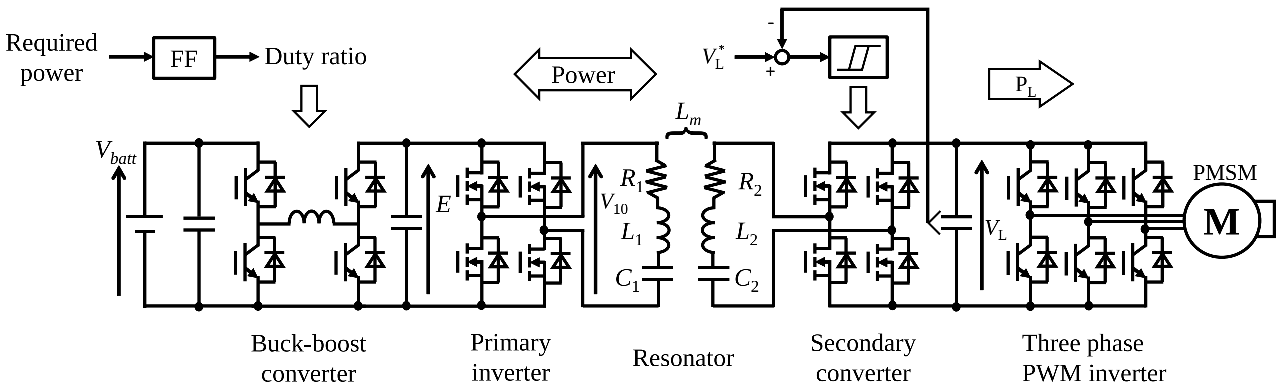

Fig. 3. Circuit configuration

Table 1. Final target and first target of car performance

	Final target	First target
Number of in-wheel motor	4	2
Maximum output power [kW]	48	6.6
Maximum wheel torque [Nm]	1300	475

verter is used instead of a diode bridge and a DC-DC converter in the W-IWM. Theoretical formulas of the W-IWM are introduced in this paper. The feasibility is demonstrated with experiment using a motor bench set.

2. Outline of the W-IWM

2.1 Target Specification As shown in Fig. 1, power and signal cables are removed. The possibility of disconnection is eliminated in this system. It is also possible to directly power the IWM wirelessly from coils under the ground. The W-IWM is installed on an experimental EV, FPEV4-*Sawyer*, developed by our research group [13] and shown in Fig. 2(a). This experimental car is composed of three parts, front/rear sub-units and the main frame. By exchanging these sub-units, the performance of various configurations can be compared as using the same platform. Fig. 2(b) shows first trial sub-unit for W-IWM. Table 1 illustrates final and first target of W-IWM. The final objective is a 48 kW output system for four wheels, however, at this stage, the authors are targeting a 6.6 kW output system for two wheels. Gap between two coils is 100 mm, considering the space between the wheel and the car body.

2.2 Circuit Configuration The circuit configuration of W-IWM is shown in Fig. 3. The required input voltage of the primary inverter changes with the output of the IWM and the misalignment of transmitter and receiver coils by the suspension stroke. The output voltage of the battery changes with the state of charge. Considering these points, a buck-boost converter is inserted on the input side of the primary inverter. Battery voltage is converted to the required voltage by controlling the buck-boost converter. DC power from the buck-boost converter is converted to high frequency AC by the primary inverter. The primary inverter is operated as a square wave inverter in this paper, but it is also possible to use the inverter as a PWM inverter. The AC power is transmitted to the secondary side circuit by magnetic resonance coupling, and rectified to DC power by the secondary converter. The DC power drives the IWM via a voltage type three-phase PWM inverter. Here, primary and secondary indicate on-board side and in-wheel side respectively. Regeneration becomes possible when the secondary converter and the primary inverter are used as an inverter and a converter respectively.

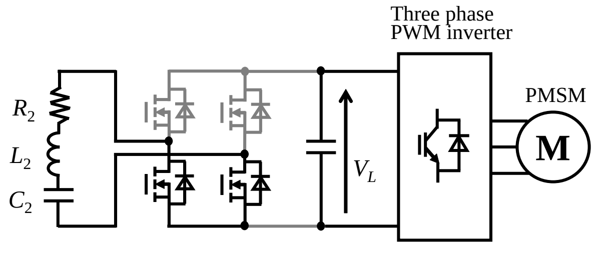

(a) Short mode

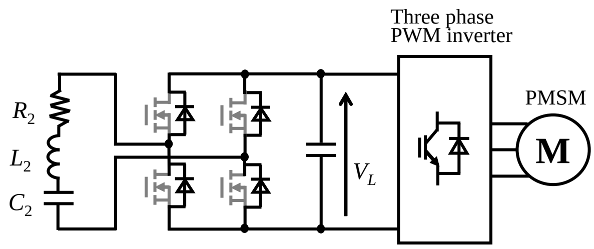

(b) Rectification mode

Fig. 4. Operation pattern of a secondary circuit

2.3 WPT via Magnetic Resonance Coupling In magnetic resonance coupling, a capacitor is inserted along with the inductor which is used for WPT to harmonize the resonance frequency of the primary and secondary circuits.

$$\omega_0 = \frac{1}{\sqrt{L_1 C_1}} = \frac{1}{\sqrt{L_2 C_2}}. \tag{1}$$

ω_0 is the operating frequency of primary inverter. L_1 and L_2 are the primary and secondary inductance, and C_1 and C_2 are the primary and secondary capacitance. The authors call this LC circuit as the resonator in this paper.

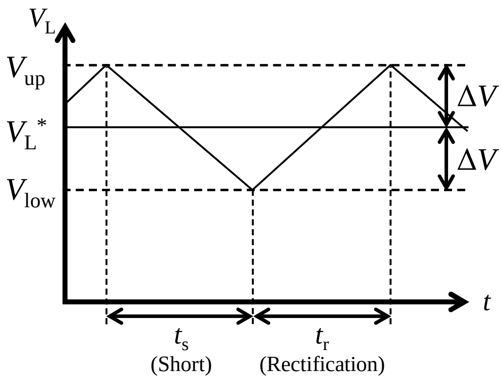

Fig. 5. A waveform of load voltage

3. Circuit Operation of W-IWM

3.1 Load Voltage Control by Hysteresis Comparator It is analyzed that the load voltage becomes unstable when a power constant load is connected to the secondary side circuit [14]. Thus, the load voltage V_L must be stabilized by feedback control. Two methods were proposed to stabilize the load voltage [6] [7]. One uses a hysteresis comparator and another uses PWM.

The method using a hysteresis comparator is applied in this paper. In the load voltage control using a hysteresis comparator, the upper side switching elements of the secondary converter are always turned off and the lower side switching elements are turned on and off. The lower and upper thresholds of the hysteresis comparator, V_{low} and V_{up}, are defined as

$$V_{low} = V_L{}^* - \Delta V \tag{2}$$

$$V_{up} = V_L{}^* + \Delta V, \tag{3}$$

where $V_L{}^*$ and ΔV are the load voltage reference and hysteresis bandwidth, respectively.

The lower-side switching elements are turned on when V_L rises over V_{up}. The state of the secondary circuit is as such shown in Fig. 4(a) (Short mode) at this time. Then, power transfer to the motor is cut off, and V_L is lowered.

The lower side switching elements are turned off when V_L falls under V_{low}. The state of the secondary circuit is shown in Fig. 4(b) (Rectification mode) at this time. Electrical power is supplied to the motor, and V_L rises if transmitted power exceeds load power.

By repeating the circuit operation mentioned above, V_L is controlled around $V_L{}^*$, as shown in Fig. 5.

3.2 Primary Voltage Control The load current changes according to the motor output when the load voltage is controlled to be a constant value. Thus, the voltage type three-phase PWM inverter and the IWM can be projected as a variable resistance load. In WPT, it is known that the electric power transmitted to secondary side changes as the load resistance value changes when a constant voltage source is connected to the primary side. Therefore, the output voltage of primary buck-boost converter is controlled with a feed-forward loop by calculating the required power on the secondary side from the torque command and the speed of the motor. It is possible to control the output voltage with a feed-forward loop by changing the duty cycle of the primary inverter. However, the authors mainly deal with the primary voltage control using the buck-boost converter in this paper.

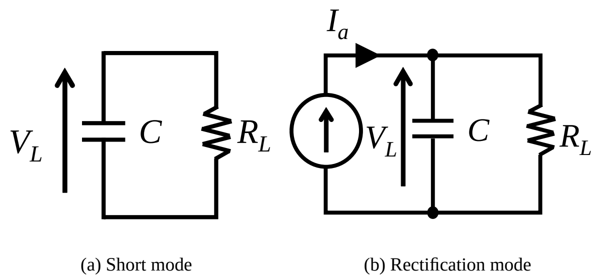

Fig. 6. A equivalent secondary circuit

4. Theoretical Power Transfer Efficiency

4.1 Changes in Transferred Power depending on the Secondary Converter Operation When the operation modes of the secondary converter are as those in Fig. 4(a) and Fig. 4(b), the rms values of the primary current are calculated as below [15].

$$I_{1s} \simeq \frac{R_2 V_{10}}{R_1 R_2 + (\omega_0 L_m)^2}, \tag{4}$$

$$I_{1r} \simeq \frac{R_2 V_{10} + \frac{2\sqrt{2}}{\pi}\omega_0 L_m V_L}{R_1 R_2 + (\omega_0 L_m)^2}. \tag{5}$$

R_1 and R_2 are the resistances of the coils. L_m is the mutual inductance between the transmitter and the receiver. V_{10} is the rms value of the fundamental harmonic in the output voltage of the primary inverter. The Fourier transform, V_{10} can be expressed as

$$V_{10} = \frac{2\sqrt{2}}{\pi} V_1, \tag{6}$$

where V_1 is rms output voltage of the primary inverter.

Hence, when the operation modes of the secondary converter are Fig. 4(a) and Fig. 4(b), the output power of the primary inverter is calculated as

$$P_{1s} \simeq \frac{R_2 V_{10}{}^2}{R_1 R_2 + (\omega_0 L_m)^2}, \tag{7}$$

$$P_{1r} \simeq \frac{R_2 V_{10} + \frac{2\sqrt{2}}{\pi}\omega_0 L_m V_L}{R_1 R_2 + (\omega_0 L_m)^2} V_{10}. \tag{8}$$

That is, the primary output power changes depending on the operation modes of the secondary converter.

4.2 Average Value of Primary Output Power In this section, the average value of the primary output power is calculated to define the power transfer efficiency when a hysteresis comparator is used in the secondary circuit. The time ratio of the short mode in one cycle of the short mode and the rectification mode is defined as

$$m_p = \frac{t_s}{t_s + t_r}. \tag{9}$$

Here, t_s and t_r are the time width of the short mode and the rectification mode in the cycle, respectively. P_1 is defined as

$$P_1 = m_p P_{1on} + (1 - m_p) P_{1off}$$

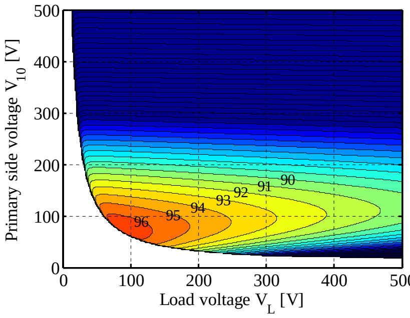

(a) P_L = 200 W

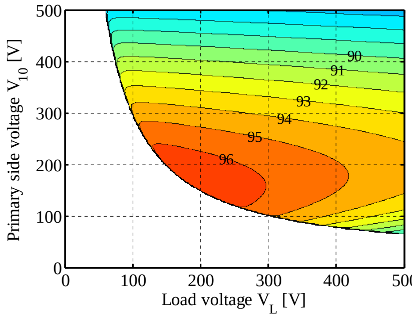

(b) P_L = 1000 W

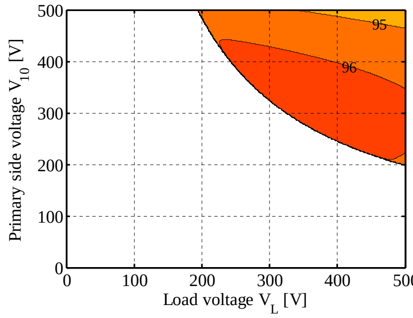

(c) P_L = 3300 W

Fig. 7. Transition of power efficiency η with changing load power P_L

$$= \frac{R_2{V_{10}}^2 + \frac{2\sqrt{2}}{\pi}\omega_0 L_m(1-m_p)V_{10}V_L}{R_1R_2 + (\omega_0 L_m)^2}. \tag{10}$$

4.3 Theoretical Formula of m_p As shown in Fig. 3, the load power is defined as P_L. The load resistance R_L is calculated by assuming that the load is regarded as a resistance.

$$R_L = \frac{{V_L}^2}{P_L} \tag{11}$$

Therefore, the secondary circuit is assumed to be Fig. 6(a) and Fig. 6(b), depending on the operation mode of the secondary converter.

By solving the circuit equation in Fig. 6(a), V_L is calculated as

$$V_L(t) = V_{\mathrm{up}}\exp\left(-\frac{1}{R_L C}t\right). \tag{12}$$

Here, t = 0 is the time at which V_L is equal to V_{up}. The secondary circuit switches to Fig. 6(b) when t is equal to t_{r}, and V(t_{r}) is equal to V_{low} at this point. Thus, t_{r} is calculated as following,

$$t_{\mathrm{r}} = R_L C \ln\left(\frac{V_{\mathrm{up}}}{V_{\mathrm{low}}}\right). \tag{13}$$

Next, by solving the circuit equation in Fig. 6(b), V_L is calculated as

$$V_L(t) = R_L I_a + (V_{\mathrm{low}} - R_L I_a)\exp\left(-\frac{1}{R_L C}t\right). \tag{14}$$

Here, t = 0 is the time at which V_L is equal to V_{low}. The secondary circuit switches to Fig. 6(a) when t is equal to t_{s}, and V(t_{s}) is equal to V_{up} at this point. Thus, t_{s} is calculated as the following,

$$t_{\mathrm{s}} = R_L C \ln\left(\frac{V_{\mathrm{low}} - R_L I_a}{V_{\mathrm{up}} - R_L I_a}\right). \tag{15}$$

In conclusion, the theoretical formula of m_p is

$$m_p = \frac{\ln\left(\frac{V_{\mathrm{low}}}{V_{\mathrm{up}}}\right)}{\ln\left(\frac{V_{\mathrm{low}}}{V_{\mathrm{up}}}\right) + \ln\left(\frac{V_{\mathrm{up}} + R_L I_a}{V_{\mathrm{low}} - R_L I_a}\right)}. \tag{16}$$

The output current of the secondary converter I_a in Fig. 6(b) is equals to the average value of the rectified current of the secondary resonator in Fig. 4(b). The rms value of the secondary resonator current $I_{2\mathrm{r}}$ is calculated as below.

$$I_{2\mathrm{r}} \simeq \frac{\omega_0 L_m V_{10} - \frac{2\sqrt{2}}{\pi}R_1 V_L}{R_1 R_2 + (\omega_0 L_m)^2} \tag{17}$$

Therefore, assuming that $I_{2\mathrm{r}}$ is a sinusoidal wave current, I_a is calculated as

$$I_a = \frac{2\sqrt{2}}{\pi}\frac{\omega_0 L_m V_{10} - \frac{2\sqrt{2}}{\pi}R_1 V_L}{R_1 R_2 + (\omega_0 L_m)^2}. \tag{18}$$

4.4 Power Transfer Efficiency From Eq. (10), the power transfer efficiency from a primary inverter output to a secondary converter is

$$\eta = \frac{\{R_1R_2 + (\omega_0 L_m)^2\}P_L}{\{R_2{V_{10}}^2 + \frac{2\sqrt{2}}{\pi}\omega_0 L_m(1-m_p)V_{10}V_L\}}. \tag{19}$$

m_p is regarded as a function of V_{10} and V_L from Eq. (11), Eq. (16) and Eq. (18). Thus, η is also regarded as a function of V_{10} and V_L from Eq. (19). Figure 7 shows the efficiency calculated from Eq. (19) with changing V_{10} and V_L in case P_L are 200 W, 1000 W and 3300 W. In all cases, there are combinations of V_{10} and V_L which maximize power transfer efficiency.

The W-IWM cannot be driven if the desired value of the load voltage is not achieved when the secondary converter is operated in rectification mode. Thus, the minimum primary voltage $V_{1\mathrm{min}}$ to attain a certain load voltage is introduced by analyzing the circuit assuming the secondary converter to be a full wave rectifier. It is calculated as

$$V_{1\mathrm{min}} = \frac{\pi}{2\sqrt{2}}\frac{\frac{8}{\pi^2}R_1R_L + R_1R_2 + (\omega_0 L_m)^2}{\omega_0 L_m R_L}V_L. \tag{20}$$

In Fig. 7, the white part indicates the range that cannot attain the required power in the secondary circuit. In this area, $V_{1\mathrm{min}} > V_{10}$ is consisted.

$\omega_0 L_m \gg R_1 \simeq R_2$ is obtained from the transmitter and receiver coils which are used in this paper. Thus, $V_{1\mathrm{min}}$ can be expressed as

$$V_{1\mathrm{min}} \simeq \frac{\pi}{2\sqrt{2}}\omega_0 L_m \frac{P_L}{V_L}. \tag{21}$$

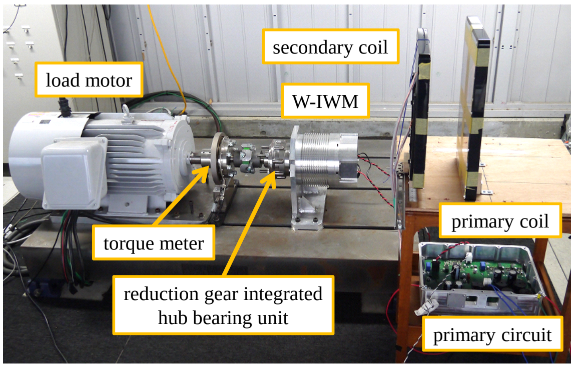

Fig. 8. An experimental bench measurement

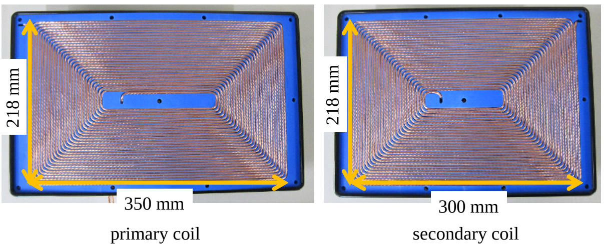

Fig. 9. Coils for WPT

Table 2. Parameters of Resonator

Parameter	Primary	Secondary
Coil resistance $R_{1,2}$	0.411 Ω	0.382 Ω
Coil inductance $L_{1,2}$	260 μH	223 μH
Capacitance $C_{1,2}$	13.5 nF	15.7 nF
Mutual inductance L_m	48.6 μH (gap: 100 mm)	
Operating frequency	83.3 kHz	

where first and second items in eq. (20) are ignored. Therefore, the boundary line of V_{10} between the color and the white regions in Fig. 7 is inversely proportional to V_L

5. Basic Experiment

5.1 Experimental Set The experimental set and the parameters of the resonator are shown in Fig. 8 and Tab. 2, respectively. Figure 9 shows the configuration of the coils, which are made by litz wires and ferrite [5]. The rectified three-phase 200 V AC is used instead of a battery as the power source. The resonant frequency is 85 kHz, which is stated as the nominal frequency by the Society of Automotive Engineers (SAE) [16]. Similarly to being mounted on an EV, the gap between the transmitter and the receiver is set to 100 mm. Switching elements in the primary inverter and the secondary converter are SiC-MOSFETs(made by ROHM, BSM180D12P2C101) [17].

5.2 Comparison of Theoretical and Experimental Values of m_p The theoretical values of m_p were compared to the experimental values. In this experiment, the W-IWM had been supplied with 30 % of the rated torque value while the revolution speed of the load motor was set to 68 rpm. The output torque was 64 Nm, and the load power P_L was 562 W. While changing primary voltage, m_p was measured at this point. V_L^* and ΔV were set as 240 V and 2.5 V, respectively. Figure 10 shows the measurement result of the secondary resonator voltage. The voltage becomes nearly zero when the lower-side switching elements of the secondary converter are turned on in Fig. 10. Thus, t_s is this time width and t_r is the other as shown in Fig. 10. The experimental value of m_p, calculated by Eq. (9) is defined as the average of ten periods. On the other hand, the theoretical value is calculated by Eq. (16).

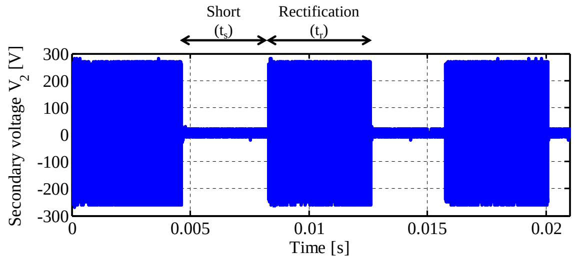

Fig. 10. A waveform of a secondary resonator

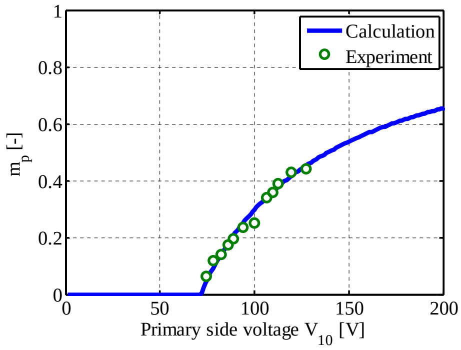

Fig. 11. A comparison with theoretical and experiment value of m_p

Comparison of the theoretical and experimental values are shown in Fig. 11. V_{10} is calculated by Eq. (6) by measuring the output voltage of the primary inverter V_1. The W-IWM cannot be driven in the range where m_p is equals to zero because V_{10} becomes lower than $V_{1\min}$. Therefore, experiments were not performed in this range. The validity of the theoretical formula is verified by the experiment.

5.3 Transition of Power Transfer Efficiency with changing V_{10} Theoretical values of η were compared to the experimental values with the changing V_{10}. In this experiment, the W-IWM was supplied with 10 % and 30 % of the rated torque value while the revolution speed of the load motor was set to 68 rpm. The output torque was 19 Nm and 64 Nm, and the load power P_L was 188 W and 562 W, respectively. By changing the primary voltage, efficiency from primary inverter output to the secondary converter output η was measured at these points. V_L^* and ΔV were set as 240 V and 2.5 V.

Comparison of the theoretical and experimental values are shown in Fig. 12. The theoretical value is calculated by eq. (19), but the losses of the secondary converter is ignored in this formula. Thus, the experimental average efficiency of the secondary converter is multiplied by the theoretical value in Fig. 12.

The theoretical primary voltage maximizing the transfer efficiency agrees with the experimental value. The errors between the calculation and the experiment are probably due to the wiring inductance and resistance.

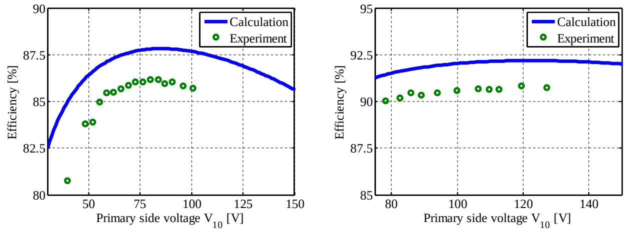

(a) T=10 % N = 68 rpm

(b) T=30 % N = 68 rpm

Fig. 12. Power transfer efficiency with changing V_1

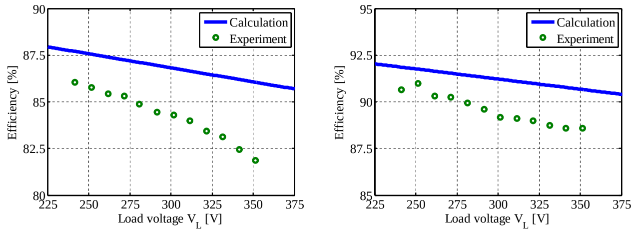

(a) T=10 % N = 68 rpm

(b) T=30 % N = 68 rpm

Fig. 13. Power transfer efficiency with changing V_L

5.4 Transition of Power Transfer Efficiency with changing V_L Theoretical values of η were compared to the experimental values with changing V_L. In this experiment, the conditions of the motor output are the same of Sec. 5.3. By varying the load voltage V_L from 240 V to 350 V, in steps of 10 V, the efficiency from the primary inverter output to the secondary converter output η was measured at these points. The primary voltage is 85 V with 10 % torque command and 122 V in 30 % torque command. These voltage values are the points where the efficiency has the maximum in Fig. 12.

Comparison of the theoretical and experimental values are shown in Fig. 13. Similar to Seq. 5.3, the experimental average efficiency of the secondary converter is multiplied by the theoretical value in Fig. 13. The theoretical load voltage maximizing the transfer efficiency agrees with experimental value as well as Sec. 5.3.

6. Conclusion

In this paper, the outline of the Wireless In-Wheel Motor using manetic resonance coupling is explained. In this system, a full bridge converter is used as the AC-DC converter in the receiver circuit. For load voltage control, the upper-side switching elements of the converter are always turned off and the lower-side switching elements are turned on and off. The power transfer efficiency in the system is demonstrated. It is revealed that there is a combination of the primary and the load voltage which maximizes the efficiency. The effectiveness of the theoretical formula of the efficiency is also shown, according to the experiment performed with bench set. The theoretical primary and load voltage maximizing transfer efficiency agrees with experimental value.

Future work includes the control of the primary and load voltage maximizing the efficiency in real time.

Acknowledgment

The research presented in this paper was funded in part by the Ministry of Education, Culture, Sports, Science and Technology grant (No. 26249061). The authors would like to express their deepest appreciation to the Murata Manufacturing Co., Ltd. for providing the laminated ceramic capacitors (U2J characteristics) used in these experiments.

References

(1) Y. Hori: "Future Vehicle Driven by Electricity and Control Research on Four Wheel Motored"UOT Electric March II"", IEEE Trans. IE, Vol. 51, No. 5, pp. 954–962 (2004)
(2) M. Suzuki, K. Sakai, K. Okada, and Y. Makino: "Development of In-Wheel Motor Type Axle Unit", NTN TECHNICAL REVIEW, No75, pp. 46–52 (2007) (in Japanese)
(3) Ntn corporation, WO2013108546 A1 (2013)
(4) Toyota Motor Corporation, P2012-223041A (2012) (in Japanese)
(5) G. Yamamoto, T. Imura, H. Fujimoto: "Transmitting and Receiving Coil Design for Wireless Power Transfer to In-Wheel Motor", IEEJ, IIC-14-073/MEC14-061, pp. 103–108 (2014) (in Japanese)
(6) D. Gunji, T. Imura, H. Fujimoto: "Fundamental Research of Power Conversion Circuit Control for Wireless In-Wheel Motor using Magnetic Resonance Coupling", IEEE IECON2014, 40th Annual Conference of the IEEE Industrial Electronics Society, pp. 3004–3009 (2014)
(7) M. Sato, G. Yamamoto, D. Gunji, T. Imura, and H.Fujimoto: "Development of Wireless In-Wheel Motor based on Magnetic Resonance Coupling," 2013 JSAE Annual Congress (Autumn), No. 113-14, pp. 9–12 (2014) (in Japanese)
(8) A. Kurs, A. Karalis, R. Moffatt, J. D. Joannopoulos, P. Fishe, and M. Soljacic: "Wireless Power Transfer via Strongly Coupled Magnetic Resonances", in Science Express on 7 June 2007, Vol.317, No.5834, pp. 83–86 (2007)
(9) T. Imura, H. Okabe, T. Uchida, and Y. Hori:"Wireless Power Transfer during Displacement Using Electromagnetic Coupling in Resonance " Magnetic-versus Electric-Type Antennas" ", IEEJ Trans. IA,Vol.130, No.1, pp. 76–83 (2010) (in Japanese)
(10) K. Iimura, N. Hoshi, and J. Haruna:"Experimental Discussion on Inductive Type Contactless Power Transfer System with Boost or Buck Converter Connected to Rectifier," Power Electronics and Motion Control Conference (IPEMC), 2012 7th International, Vol. 4, pp. 2652–2657 (2012)
(11) M. Kato, T. Imura, and Y. Hori, "Study on Maximize Efficiency by Secondary Side Control Using DC-DC Converter in Wireless Power Transfer via Magnetic resonant Coupling," in IEEE EVS27 Internatonal Battery, Hybrid and Fuel Cell Electric Vehicle Symposium (2013)
(12) W. Zhong, and S. Y. R. Hui:"Maximum Energy Efficiency Tracking for Wireless Power Transfer Systems", Power Electronics, IEEE Transactions on (2014)
(13) H. Fujimoto, T. Miyajima, and J. Amada: "Development of Electric Vehicle with Variable Drive Unit System", International Electric Vehicle Technology Conference & Automotive Power Electronics Japan 2014 (2014)
(14) D. Gunji, T. Imura, and H. Fujimoto"Stability Analysis of Secondary Load Voltage on Wireless Power Transfer using Magnetic Resonance Coupling for Constant Power Load", IEE of Japan Industry Applications Society Conference, No.3-42, pp.251–254 (2014) (in Japanese)
(15) D. Gunji, T. Imura, H. Fujimoto: "Basic Study of Transmitting Power Control Method without Signal Communication on Wireless Power Transfer", IEEJ, SPC-14-153,HCA-14-061,VT-14-048 (2014) (in Japanese)
(16) SAE International: "Wireless charging advances with selection of 85-kHz charging frequency", http://articles.sae.org/12647/ (2013)
(17) ROHM: "SiC Power Module BSM180D12P2C101 Datasheet" (2013)